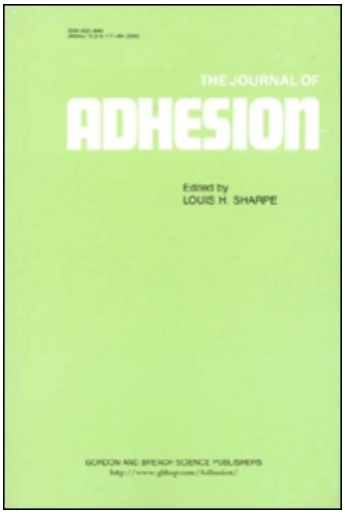

The Journal of Adhesion

Publication details, including instructions for authors and subscription information:
http://www.informaworld.com/smpp/title~content=t713453635

A Two-dimensional Stress Analysis and Strength of Single-lap Adhesive Joints of Dissimilar Adherends Subjected to External Bending Moments

Jiemin Liu[a]; Toshiyuki Sawa[a]; Hiroshi Toratani[a]
[a] Department of Mechanical Engineering, Yamanashi University, Kofu, Yamanashi, Japan

To cite this Article Liu, Jiemin , Sawa, Toshiyuki and Toratani, Hiroshi(1999) 'A Two-dimensional Stress Analysis and Strength of Single-lap Adhesive Joints of Dissimilar Adherends Subjected to External Bending Moments', The Journal of Adhesion, 69: 3, 263 — 291
To link to this Article: DOI: 10.1080/00218469908017231
URL: http://dx.doi.org/10.1080/00218469908017231

J. Adhesion, 1999, Vol. 69, pp. 263–291
Reprints available directly from the publisher
Photocopying permitted by license only

A Two-dimensional Stress Analysis and Strength of Single-lap Adhesive Joints of Dissimilar Adherends Subjected to External Bending Moments

JIEMIN LIU, TOSHIYUKI SAWA* and HIROSHI TORATANI

Department of Mechanical Engineering, Yamanashi University, 4-3-11, Takeda, Kofu, Yamanashi, 400 Japan

(Received 5 May 1998; In final form 19 October 1998)

The stress distributions of single-lap adhesive joints of dissimilar adherends subjected to external bending moments are analyzed as a three-body contact problem by using a two-dimensional theory of elasticity (plane strain). In the analysis, dissimilar adherends and an adhesive are replaced by finite strips. In the numerical calculations, the effects of the ratio of Young's moduli of adherends, the adherend thickness ratio and the adherend length ratio between dissimilar adherends on the stress distributions at the interfaces are examined. The results show that the stress singularity occurs at the ends of the interfaces, and its intensity is greater at the interface of the adherend with smaller Young's modulus. It is also noted that the singular stress is greater at the interface of the thinner adherend. It is found that the effect of the adherend length ratio on the stress singularity at the interfaces is very small. Joint strength is predicted by using the interface stress and it was measured by experiments. From the analysis and the experiments, it is found that the joint strength increases as Young's modulus of adherends and the adherend thickness increase while the effect of the adherend lengths on the joint strength is small. For verification of the analysis, a finite element analysis (FEA) is carried out. A fairly good agreement of the interface stress distribution is seen between the analytical and the FEA results.

Keywords: Stress analysis; single-lap joint; adhesive; dissimilar adherends; bending moment; interface; theory of elasticity; singular stress; joint strength; two-dimension; plane strain

* Corresponding author. Tel.: +81552-20-8438, Fax: +81552-20-8438.

1. INTRODUCTION

Single-lap adhesive joints have been widely used in the mechanical, automobile and aerospace industries, and so on, as the performance of adhesives has been developed. However, they have not been used in the principal parts of structures because of the large deviation in joint strength. In the design of adhesive joints, it is important to know the stress distributions in the joints, especially at the interfaces between the adherends and the adhesive. Many investigations have been carried out on single-lap [1–8], double-lap [9], scarf [10] and butt [11–13] adhesive joints subjected to tensile loads, experimentally [3, 5], by the methods of mechanics of materials [1, 7], by finite element methods [4, 9] and by the two-dimensional theory of elasticity [2, 8–13]. In practice, single-lap adhesive joints of dissimilar adherends have been used and they are sometimes subjected to external bending moments. Few researches [14, 15] have been performed on single-lap adhesive joints of similar adherends subjected to external bending moments. In establishing an optimal design of adhesive jonts, it is necessary to know the stress distribution of single-lap adhesive joints of dissimilar adherends subjected to external bending moments. These external bending moments are quite different from those that occur in single-lap adhesive joints subjected to tensile loads.

In this paper, the stress distributions of single-lap adhesive joints of dissimilar adherends subjected to external bending moments are analyzed as a three-body contact problem by using a two-dimensional theory of elasticity (plane strain state). In the numerical calculations, the effects of the ratio of Young's moduli among adherends and an adhesive, the adherend thickness ratio and the adherend length ratio between dissimilar adherends on the stress distributions at the interfaces are examined. For verification of the analysis, a two-dimensional finite element analysis (FEA) of single-lap adhesive joints of dissimilar adherends subjected to external bending moments is conducted. Comparisons between the numerical and the FEA results are made. In addition, using the interface stress distribution, joint strength is predicted. Experiments to measure the strain and joint strength were performed. Comparisons of the strain and joint strength are made between the numerical and the experimental results.

2. THEORETICAL ANALYSIS

Figure 1(a) shows a single-lap adhesive joint of dissimilar adherends subjected to an external bending moment $M(= (W/2) \times a)$. Figure 1(b) shows a model for the analysis. In Figure 1(b), the upper and lower adherends are replaced by finite strips [I] and [III], and the adhesive by finite strip [II]. The origins of the finite strips [I], [II] and [III] are denoted by O_1, O_2 and O_3, and the corresponding coordinates are chosen as $(x_1, y_1), (x_2, y_2)$ and (x_3, y_3), respectively. The length and height of finite strip [I] are designated as $2l_1$, and $2h_1$, and Young's modulus and Poisson's ratio as E_1 and ν_1 respectively. Those for finite strips [II] and [III] are designated as $2l_2, 2h_2, E_2, \nu_2, 2l_3, 2h_3, E_3$ and ν_3, respectively. A bending moment, M, is assumed to be applied as the

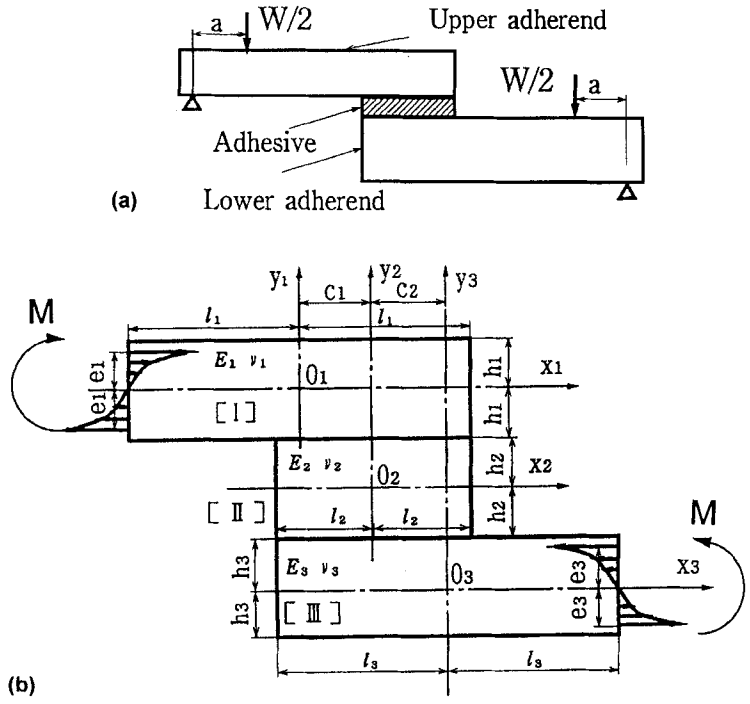

FIGURE 1 Single-lap adhesive joint of dissimilar adherends subjected to an external bending moment (a) A single-lap adhesive joint subjected to four-point bending moments; (b) A model for analysis.

stress distribution $F(y_1)$ in the region $x_1 = -l_1$, $|y_1| \leqq e_1$, and $F(y_3)$ in the region $x_1 = l_3$, $|y_3| \leqq e_3$ as shown in Figure 1(b). Figure 2 shows the dimensions and the assumed stress distributions for each finite strip. In this analysis, for simplicity, the stress distributions $F(y_1)$ and $F(y_3)$ are assumed to be linear and the absolute values at the positions $y_1 = \pm h_1$ and $y_3 = \pm h_3$ are denoted as p_1 and p_3 as shown in Figure 2(a) and (c). Expanding the stress distributions $F(y_1)$ and $F(y_3)$ into Fourier series, the boundary conditions are expressed as Eqs. (1) to (3), and the contact conditions at the upper and lower interfaces are expressed as Eqs. (4) and (5), respectively, where the displacement in the x direction is denoted as u and the displacement in the y direction as v. In addition, the superscripts I, II and III of the stress and displacement components in Eqs. (1) to (5) describe finite strips [I], [II] and [III], respectively.

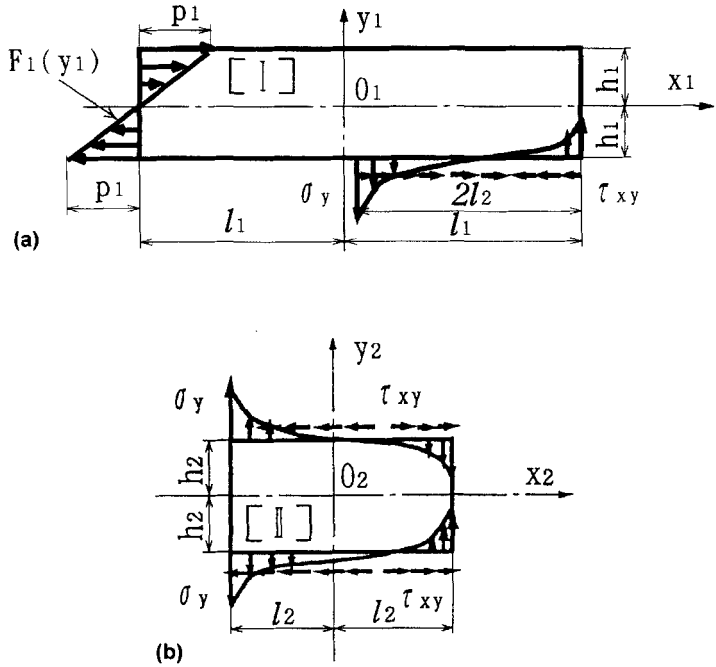

FIGURE 2 Dimensions and assumed stress distributions of each finite strip, (a) finite strip [I] (upper adherend); (b) finite strip [II] (adhesive); (c) finite strip [III] (lower adherend).

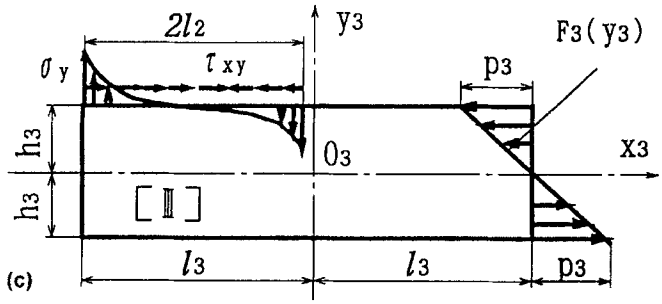

FIGURE 2 (Continued).

(a) For finite strip [I] (upper adherend)

$$\begin{aligned}
x_1 = l_1: &\quad \sigma_x^{\mathrm{I}} = 0; \quad \tau_{xy}^{\mathrm{I}} = 0 \\
x_1 = -l_1: &\quad \sigma_x^{\mathrm{I}} = F(y_1) = \Sigma b_s^{\mathrm{I}} \sin((2s-1)\pi x_1/(2h_1)) \\
&\quad \tau_{xy}^{\mathrm{I}} = 0 \\
y_1 = h_1: &\quad \sigma_y^{\mathrm{I}} = 0; \quad \tau_{xy}^{\mathrm{I}} = 0 \\
y_1 = -h_1: &\quad \sigma_y^{\mathrm{I}} = 0; \quad \tau_{xy}^{\mathrm{I}} = 0 \quad (-l_1 \leqq x_1 \leqq c_1 - l_2)
\end{aligned} \tag{1}$$

(b) For finite strip [II] (adhesive)

$$\begin{aligned}
x_2 = l_2: &\quad \sigma_x^{\mathrm{II}} = 0; \quad \tau_{xy}^{\mathrm{II}} = 0 \\
x_2 = -l_2: &\quad \sigma_x^{\mathrm{II}} = 0; \quad \tau_{xy}^{\mathrm{II}} = 0
\end{aligned} \tag{2}$$

(c) For finite strip [III] (lower adherend)

$$\begin{aligned}
x_3 = -l_3: &\quad \sigma_x^{\mathrm{III}} = 0; \quad \tau_{xy}^{\mathrm{III}} = 0 \\
x_3 = -l_3: &\quad \sigma_x^{\mathrm{III}} = F(y_3) = \sum b_s^{\mathrm{III}} \sin((2s-1)\pi x_3/(2h_3)) \\
&\quad \tau_{xy}^{\mathrm{III}} = 0 \\
y_3 = -h_3: &\quad \sigma_y^{\mathrm{III}} = 0; \quad \tau_{xy}^{\mathrm{III}} = 0 \\
y_3 = h_3: &\quad \sigma_y^{\mathrm{III}} = 0; \quad \tau_{xy}^{\mathrm{III}} = 0 \quad (-C_2 + l_2 \leqq x_3 \leq l_3)
\end{aligned} \tag{3}$$

(d) At the upper interface (the interface between finite strips [I] and [II])

$$
\begin{aligned}
&(\sigma_y^{\mathrm{I}})_{y_1=-h_1} = (\sigma_y^{\mathrm{II}})_{y_2=h_2} \\
&(\tau_{xy}^{\mathrm{I}})_{y_1=-h_1} = (\tau_{xy}^{\mathrm{II}})_{y_2=h_2} \\
&(u_{,x}^{\mathrm{I}})_{y_1=-h_1} = (u_{,x}^{\mathrm{II}})_{y_2=h_2} \\
&(v_{,x}^{\mathrm{I}})_{y_1=-h_1} = (v_{,x}^{\mathrm{II}})_{y_2=h_2} \\
&(c_2 - l_2 \leqq x_1 \leqq c_1 + l_2,\ c_1 = l_1 - l_2,\ |x_2| \leqq l_2,\ l_2 \leqq l_1)
\end{aligned}
\tag{4}
$$

(e) At the lower interface (the interface between finite strips [II] and [III])

$$
\begin{aligned}
&(\sigma_y^{\mathrm{II}})_{y_2=-h_2} = (\sigma_y^{\mathrm{III}})_{y_3=h_3} \\
&(\tau_{xy}^{\mathrm{II}})_{y_2=-h_2} = (\tau_{xy}^{\mathrm{III}})_{y_3=h_3} \\
&(u_{,x}^{\mathrm{II}})_{y_2=-h_2} = (u_{,x}^{\mathrm{III}})_{y_3=h_3} \\
&(v_{,x}^{\mathrm{II}})_{y_2=-h_2} = (v_{,x}^{\mathrm{III}})_{y_3=h_3} \\
&(-c_2 - l_2 \leqq x_3 \leqq -c_2 + l_2,\ c_2 = l_3 - l_2,\ |x_2| \leqq l_2,\ l_2 \leqq l_3)
\end{aligned}
\tag{5}
$$

where b_s^{I} and b_s^{III} are Fourier coefficients and they are expressed by the following equations.

$$
b_s^{\mathrm{I}} = \frac{1}{h_1} \int_{-e_1}^{e_1} F(y_1) \cdot \sin \frac{(2s-1)\pi y_1}{2h_1}\, dy_1
$$

$$
b_s^{\mathrm{III}} = \frac{1}{h_3} \int_{-e_3}^{e_3} F(y_3) \sin \frac{(2s-1)\pi y_3}{2h_3}\, dy_3
$$

In the boundary conditions, Eqs. (4) and (5), at the interfaces, the compliance conditions of the deformations are expressed by the first order partial derivative of the displacements u and v, not by the displacement u and v directly because different origins of the coordinates O_1, O_2 and O_3 are used, which is convenient for deriving the equations. It should be pointed out that the conditions shown in Eqs. (1) to (5) are mixed boundary conditions. The method of solving the mixed boundary conditions is briefly explained in the Appendix.

Airy's stress functions [9, 11] are used in order to anlyze each finite strip under the boundary conditions expressed by Eqs. (1) to (5). Stress components and displacement components expressed by Airy's stress

functions, X, in the plane stress state are shown by Eqs. (6) and (7), respectively,

$$\sigma_x = X_{,yy}\,, \quad \sigma_y = X_{,xx}\,, \quad \tau_{xy} = -X_{,xy} \tag{6}$$

$$2Gu = -X_{,x} + \phi_{,y}/(1+\nu), \quad 2Gv = -X_{,y} + \phi_{,x}/(1+\nu) \tag{7}$$

where

$$\nabla^2\nabla^2 X = 0, \quad \nabla^2\phi = 0, \quad (\nabla^2\phi = \phi_{,xx} + \phi_{,yy})$$

and the relationship between ϕ and X is expressed by Eq. (8).

$$\phi_{,xy} = \nabla^2 X \tag{8}$$

where G is shear modulus and ν is Poisson's ratio, and G is expressed by the equation $G = E/(2(1-\nu))$. The stress components in the plane strain state are obtained by changing Young's modulus E and Poisson' ratio ν into $E/(1-\nu^2)$ and $\nu/(1-\nu)$, respectively.

Airy's stress function, X^{I}, for analyzing finite strip [I] is expressed by Eqs. (9) and (10). Airy's stress functions, X^{III} for analyzing finite strip [III] are similar to X^{I} and can be easily obtained by changing the subscript "I" and the subscript "1" expressed in Eqs. (9) and (10) into "III" and "3", respectively.

$$X^{\mathrm{I}} = \chi_1^{\mathrm{I}} + \chi_2^{\mathrm{I}} + \chi_3^{\mathrm{I}} + \chi_4^{\mathrm{I}} + \chi_5^{\mathrm{I}} + \chi_6^{\mathrm{I}} + \chi_7^{\mathrm{I}} + \chi_8^{\mathrm{I}} \tag{9}$$

where

$$\begin{aligned}
\chi_1^{\mathrm{I}} &= \chi_1\left(A_{n1}^{\mathrm{I}}, B_{s1}^{\mathrm{I}}, l_1, h_1, \alpha_n^{\mathrm{I}}, \lambda_s^{\mathrm{I}}, \Delta_{n1}^{\mathrm{I}}, \Omega_{s1}^{\mathrm{I}}, x_1, y_1\right) \\
&= \sum_{n=1}^{\infty} \frac{A_{n1}^{\mathrm{I}}}{\Delta_{n1}^{\mathrm{I}}\alpha_n^{\mathrm{I}^2}} \left[\left(\alpha_n^{\mathrm{I}} l_1 \cos h(\alpha_n^{\mathrm{I}} l_1) + \sin h(\alpha_n^{\mathrm{I}} l_1)\right)\cos h(\alpha_n^{\mathrm{I}} x_1)\right. \\
&\quad \left. - \alpha_n^{\mathrm{I}} x_1 \sin h(\alpha_n^{\mathrm{I}} l_1)\sin h(\alpha_n^{\mathrm{I}} x_1)\right]\cos(\alpha_n^{\mathrm{I}} y_1) \\
&\quad + \sum_{s=1}^{\infty} \frac{B_{s1}^{\mathrm{I}}}{\Omega_{s1}^{\mathrm{I}}\lambda_s^{\mathrm{I}^2}} \left[\left(\lambda_s^{\mathrm{I}} h_1 \cos h(\lambda_s^{\mathrm{I}} h_1) + \sin h(\lambda_s^{\mathrm{I}} h_1)\right)\cos h(\lambda_s^{\mathrm{I}} y_1)\right. \\
&\quad \left. - \lambda_s^{\mathrm{I}} y_1 \sin h(\lambda_s^{\mathrm{I}} h_1)\sin h(\lambda_s^{\mathrm{I}} y_1)\right]\cos(\lambda_s^{\mathrm{I}} x_1)
\end{aligned} \tag{10.1}$$

$$\chi_2^{\mathrm{I}} = \chi_2(A_{n2}^{\mathrm{I}}, B_{s2}^{\mathrm{I}}, l_1, h_1, \alpha_n^{\mathrm{I}'}, \lambda_s^{\mathrm{I}}, \Delta_{n2}^{\mathrm{I}}, \Omega_{s2}^{\mathrm{I}}, x_1, y_1)$$

$$
\begin{aligned}
&= \sum_{n=1}^{\infty} \frac{A_{n2}^{\mathrm{I}}}{\Delta_{n2}^{\mathrm{I}}(\alpha_n^{\mathrm{I}'})^2} [(\alpha_n^{\mathrm{I}'} l_1 \cos h(\alpha_n^{\mathrm{I}'} l_1) + \sin h(\alpha_n^{\mathrm{I}'} l_1)) \cos h(\alpha_n^{\mathrm{I}'} x_1) \\
&\quad - \alpha_n^{\mathrm{I}'} x_1 \cos h(\alpha_n^{\mathrm{I}'} l_1) \sin h(\alpha_n^{\mathrm{I}'} x_1)] \cos(\alpha_n^{\mathrm{I}'} y_1) \\
&\quad + \sum_{s=1}^{\infty} \frac{B_{s2}^{\mathrm{I}}}{\Omega_{s2}^{\mathrm{I}} \lambda_s^{\mathrm{I}^2}} [(\lambda_s^{\mathrm{I}} h_1 \sin h(\lambda_s^{\mathrm{I}} h_1) + \cos h(\lambda_s^{\mathrm{I}} h_I)) \sin h(\lambda_s^{\mathrm{I}} y_1) \\
&\quad - \lambda_s^{\mathrm{I}} y_1 \cos h(\lambda_s^{\mathrm{I}} h_1) \cos h(\lambda_s^{\mathrm{I}} y_1)] \cos(\lambda_s^{\mathrm{I}} x_1)
\end{aligned} \tag{10.2}
$$

$$
\begin{aligned}
\chi_3^{\mathrm{I}} &= \chi_3(A_{n3}^{\mathrm{I}}, B_{s3}^{\mathrm{I}}, l_1, h_1, \alpha_n^{\mathrm{I}'}, \lambda_s^{\mathrm{I}'}, \Delta_{n3}^{\mathrm{I}}, \Omega_{s3}^{\mathrm{I}}, x_1, y_1) \\
&= -\sum_{n=1}^{\infty} \frac{A_{n3}^{\mathrm{I}}}{\Delta_{n3}^{\mathrm{I}}(\alpha^{\mathrm{I}'_n})^2} [\alpha_n^{\mathrm{I}'} l_1 \sin h(\alpha_n^{\mathrm{I}'} l_1) \cos h(\alpha_n^{\mathrm{I}'} x_1) \\
&\quad - \alpha_n^{\mathrm{I}'} x_1 \cos h(\alpha_n^{\mathrm{I}'} l_1) \sin h(\alpha_n^{\mathrm{I}'} x_1)] \cos(\alpha_n^{\mathrm{I}'} y_1) \\
&\quad - \sum_{s=1}^{\infty} \frac{B_{s3}^{\mathrm{I}}}{\Omega_{s3}^{\mathrm{I}}(\lambda_s^{\mathrm{I}'})^2} [\lambda_s^{\mathrm{I}'} h_1 \sin h(\lambda_s^{\mathrm{I}'} h_1) \cos h(\lambda_s^{\mathrm{I}'} y_1) \\
&\quad - \lambda_s^{\mathrm{I}'} y_1 \cos h(\lambda_s^{\mathrm{I}'} h_1) \sin h(\lambda_s^{\mathrm{I}'} y_1)] \cos(\lambda_s^{\mathrm{I}'} x_1)
\end{aligned} \tag{10.3}
$$

$$
\begin{aligned}
\chi_4^{\mathrm{I}} &= \chi_4(A_{n4}^{\mathrm{I}}, B_{s4}^{\mathrm{I}}, l_1, h_1, \alpha_n^{\mathrm{I}}, \lambda_s^{\mathrm{I}'}, \Delta_{n4}^{\mathrm{I}}, \Omega_{s4}^{\mathrm{I}}, x_1, y_1) \\
&= -\sum_{n=1}^{\infty} \frac{A_{n4}^{\mathrm{I}}}{\Delta_{n4}^{\mathrm{I}}(\alpha_n^{\mathrm{I}})^2} [\alpha_n^{\mathrm{I}} l_1 \sin h(\alpha_n^{\mathrm{I}} l_1) \cos h(\alpha_n^{\mathrm{I}} x_1) \\
&\quad - \alpha_n^{\mathrm{I}} x_1 \cos h(\alpha_n^{\mathrm{I}} l_1) \sin h(\alpha_n^{\mathrm{I}} x_1)] \sin(\alpha_n^{\mathrm{I}} y_1) \\
&\quad - \sum_{s=1}^{\infty} \frac{B_{s4}^{\mathrm{I}}}{\Omega_{s4}^{\mathrm{I}}(\lambda_s^{\mathrm{I}'})^2} [(\lambda_s^{\mathrm{I}'} h_1 \cos h(\lambda_s^{\mathrm{I}'} h_1) \sin h(\lambda_s^{\mathrm{I}'} y_1) \\
&\quad - \lambda_s^{\mathrm{I}'} y_1 \sin h(\lambda_s^{\mathrm{I}'} h_1) \cos h(\lambda_s^{\mathrm{I}'} y_1)] \cos(\lambda_s^{\mathrm{I}'} x_1)
\end{aligned} \tag{10.4}
$$

$$
\begin{aligned}
\chi_5^{\mathrm{I}} &= \chi_5(A_{n5}^{\mathrm{I}}, B_{s5}^{\mathrm{I}}, l_1, h_1, \alpha_n^{\mathrm{I}}, \lambda_s^{\mathrm{I}'}, \Delta_{n5}^{\mathrm{I}}, \Omega_{s5}^{\mathrm{I}}, x_1, y_1) \\
&= -\sum_{n=1}^{\infty} \frac{A_{n5}^{\mathrm{I}}}{\Delta_{n5}^{\mathrm{I}} \alpha_n^{\mathrm{I}^2}} [(\alpha_n^{\mathrm{I}} l_1 \sin h(\alpha_n^{\mathrm{I}} l_1) + \cos h(\alpha_n^{\mathrm{I}} l_1)) \sin h(\alpha_n^{\mathrm{I}} x_1) \\
&\quad - \alpha_n^{\mathrm{I}} x_1 \cos h(\alpha_n^{\mathrm{I}} l_1) \cos h(\alpha_n^{\mathrm{I}} x_1)] \cos(\alpha_n^{\mathrm{I}} y_1) \\
&\quad + \sum_{s=1}^{\infty} \frac{B_{s5}^{\mathrm{I}}}{\Omega_{s5}^{\mathrm{I}}(\lambda_s^{\mathrm{I}'})^2} [(\lambda_s^{\mathrm{I}'} h_1 \cos h(\lambda_s^{\mathrm{I}'} h_1) + \sin h(\lambda_s^{\mathrm{I}'} h_I)) \cos h(\lambda_s^{\mathrm{I}'} y_1) \\
&\quad - \lambda_s^{\mathrm{I}'} y_1 \sin h(\lambda_s^{\mathrm{I}'} h_1) \sin h(\lambda_s^{\mathrm{I}'} y_1)] \sin(\lambda_s^{\mathrm{I}'} x_1)
\end{aligned} \tag{10.5}
$$

$$\begin{aligned}\chi_6^{\mathrm{I}} &= \chi_6(A_{n6}^{\mathrm{I}}, B_{s6}^{\mathrm{I}}, l_1, h_1, \alpha_n^{\mathrm{I}'}, \lambda_s^{\mathrm{I}'}, \Delta_{n6}^{\mathrm{I}}, \Omega_{s6}^{\mathrm{I}}, x_1, y_1)\\ &= \sum_{n=1}^{\infty} \frac{A_{n6}^{\mathrm{I}}}{\Delta_{n6}^{\mathrm{I}}(\alpha_n^{\mathrm{I}'})^2}[(\alpha_n^{\mathrm{I}'} l_1 \sin h(\alpha_n^{\mathrm{I}'} l_1) + \cos h(\alpha_n^{\mathrm{I}'} l_1)) \sin h(\alpha_n^{\mathrm{I}'} x_1)\\ &\quad - \alpha_n^{\mathrm{I}'} x_1 \cos h(\alpha_n^{\mathrm{I}'} l_1) \cos h(\alpha_n^{\mathrm{I}'} x_1)] \sin(\alpha_n^{\mathrm{I}'} y_1)\\ &\quad + \sum_{s=1}^{\infty} \frac{B_{s6}^{\mathrm{I}}}{\Omega_{s6}^{\mathrm{I}}(\lambda_s^{\mathrm{I}'})^2}[(\lambda_s^{\mathrm{I}'} h_1 \sin h(\lambda_s^{\mathrm{I}'} h_1) + \cos h(\lambda_s^{\mathrm{I}'} h_I)) \sin h(\lambda_s^{\mathrm{I}'} y_1)\\ &\quad - \lambda_s^{\mathrm{I}'} y_1 \cos h(\lambda_s^{\mathrm{I}'} h_1) \cos h(\lambda_s^{\mathrm{I}'} y_1)] \sin(\lambda_s^{\mathrm{I}'} x_1)\end{aligned} \tag{10.6}$$

$$\begin{aligned}\chi_7^{\mathrm{I}} &= \chi_7(A_{n7}^{\mathrm{I}}, B_{s7}^{\mathrm{I}}, l_1, h_1, \alpha_n^{\mathrm{I}'}, \lambda_s^{\mathrm{I}}, \Delta_{n7}^{\mathrm{I}}, \Omega_{s7}^{\mathrm{I}}, x_1, y_1)\\ &= -\sum_{n=1}^{\infty} \frac{A_{n7}^{\mathrm{I}}}{\Delta_{n7}^{\mathrm{I}}(\alpha_n^{\mathrm{I}'})^2}[\alpha_n^{\mathrm{I}'} l_1 \cos h(\alpha_n^{\mathrm{I}'} l_1) \sin h(\alpha_n^{\mathrm{I}'} x_1)\\ &\quad - \alpha_n^{\mathrm{I}'} x_1 \sin h(\alpha_n^{\mathrm{I}'} l_1) \cos h(\alpha_n^{\mathrm{I}'} x_1)] \cos(\alpha_n^{\mathrm{I}'} y_1)\\ &\quad - \sum_{s=1}^{\infty} \frac{B_{s7}^{\mathrm{I}}}{\Omega_{s7}^{\mathrm{I}} \lambda_s^{\mathrm{I}\,2}}[\lambda_s^{\mathrm{I}} h_1 \sin h(\lambda_s^{\mathrm{I}} h_1) \cos h(\lambda_s^{\mathrm{I}} y_1)\\ &\quad - \lambda_s^{\mathrm{I}'} y_1 \cos h(\lambda_s^{\mathrm{I}} h_1) \sin h(\lambda_s^{\mathrm{I}} y_1)] \sin(\lambda_s^{\mathrm{I}} x_1)\end{aligned} \tag{10.7}$$

$$\begin{aligned}\chi_8^{\mathrm{I}} &= \chi_8(A_{n8}^{\mathrm{I}}, B_{s8}^{\mathrm{I}}, l_1, h_1, \alpha_n^{\mathrm{I}}, \lambda_s^{\mathrm{I}}, \Delta_{n8}^{\mathrm{I}}, \Omega_{s8}^{\mathrm{I}}, x_1, y_1)\\ &= -\sum_{n=1}^{\infty} \frac{A_{n8}^{\mathrm{I}}}{\Delta_{n8}^{\mathrm{I}} \alpha_n^{\mathrm{I}\,2}}[\alpha_n^{\mathrm{I}} l_1 \cos h(\alpha_n^{\mathrm{I}} l_1) \sin h(\alpha_n^{\mathrm{I}} x_1)\\ &\quad - \alpha_n^{\mathrm{I}} x_1 \sin h(\alpha_n^{\mathrm{I}} l_1) \cos h(\alpha_n^{\mathrm{I}} x_1)] \sin(\alpha_n^{\mathrm{I}} y_1)\\ &\quad - \sum_{s=1}^{\infty} \frac{B_{s8}^{\mathrm{I}}}{\Omega_{s8}^{\mathrm{I}} \lambda_s^{\mathrm{I}\,2}}[\lambda_s^{\mathrm{I}} h_1 \cos h(\lambda_s^{\mathrm{I}} h_1) \sin h(\lambda_s^{\mathrm{I}} y_1)\\ &\quad - \lambda_s^{\mathrm{I}} y_1 \sin h(\lambda_s^{\mathrm{I}} h_1) \cos h(\lambda_s^{\mathrm{I}} y_1)] \sin(\lambda_s^{\mathrm{I}} x_1)\end{aligned} \tag{10.8}$$

Airy's functions, X^{II}, for analyzing finite strip [II] are expressed by Eqs. (11) and (12) using the Eq. (10).

$$X^{\mathrm{II}} = \chi_1^{\mathrm{II}} + \chi_3^{\mathrm{II}} + \chi_6^{\mathrm{II}} + \chi_8^{\mathrm{II}} \tag{11}$$

where

$$\begin{aligned}
\chi_1^{II} &= \chi_1(A_{n1}^{II}, B_{s1}^{II}, l_2, h_2, \alpha_n^{II}, \lambda_s^{II}, \Delta_{n1}^{II}, \Omega_{s1}^{II}, x_2, y_2)\\
\chi_3^{II} &= \chi_3(A_{n3}^{II}, B_{s3}^{II}, l_2, h_2, \alpha_n^{II}, \lambda_s^{II'}, \Delta_{n3}^{II}, \Omega_{s3}^{II}, x_2, y_2)\\
\chi_6^{II} &= \chi_6(A_{n6}^{II}, B_{s6}^{II}, l_2, h_2, \alpha_n^{II'}, \lambda_s^{II'}, \Delta_{n6}^{II}, \Omega_{s6}^{II}, x_2, y_2)\\
\chi_8^{II} &= \chi_8(A_{n8}^{II}, B_{s8}^{II}, l_2, h_2, \alpha_n^{II}, \lambda_s^{II}, \Delta_{n8}^{II}, \Omega_{s8}^{II}, x_2, y_2)
\end{aligned} \tag{12}$$

$A_{n1}^{I}, B_{s1}^{I}, A_{n2}^{I}, B_{s2}^{I}, A_{n3}^{I}, B_{s3}^{I}, A_{n4}^{I}, B_{s4}^{I}, A_{n5}^{I}, B_{s5}^{I}, A_{n6}^{I}, B_{s6}^{I}, A_{n7}^{I}, B_{s7}^{I}, A_{n8}^{I}$, B_{s8}^{I} (I = I, III), $A_{n2}^{II}, B_{n2}^{II}, A_{n4}^{II}, B_{n4}^{II}, A_{n5}^{II}, B_{n5}^{II}, A_{n7}^{II}$ and B_{n7}^{II} are unknown coefficients which will be determined from the boundary conditions and continuity conditions expressed by Eqs. (1) to (5), and where

$$\begin{aligned}
&\alpha_n^{I} = \frac{n\pi}{h_1},\ \alpha_n^{I'} = \frac{(2n-1)\pi}{2h_i},\ \lambda_s^{I} = \frac{s\pi}{l_i},\ \lambda_s^{I'} = \frac{(2s-1)\pi}{2l_i}\\
&\Delta_{nl}^{I} = \Delta_{n4}^{I} = \Delta_n(\alpha_n^{I} l_i) = \sin h(\alpha_n^{I} l_i)\cos h(\alpha_n^{I} l_i) + \alpha_n^{I} l_i\\
&\Delta_{n5}^{I} = \Delta_{n8}^{I} = \Delta_n^{*}(\alpha_n^{I} l_i) = \sin h(\alpha_n^{I} l_i)\cos h(\alpha_n^{I} l_i) - \alpha_n^{I} l_i\\
&\Delta_{n2}^{I} = \Delta_{n3}^{I} = \Delta_n(\alpha_n^{I'} l_i),\ \Delta_{n6}^{I} = \Delta_{n7}^{I} = \Delta_n^{*}(\alpha_n^{I'} l_i)\\
&\Omega_{s1}^{I} = \Omega_{s7}^{I} = \Omega_s(\lambda_s^{I} h_1) = \sin h(\lambda_s^{I} h_i)\cos h(\lambda_s^{I} h_i) + \lambda_s^{I} h_i\\
&\Omega_{s2}^{I} = \Omega_{s8}^{I} = \Omega_s^{*}(\lambda_s^{I} h_i) = \sin h(\lambda_s^{I} h_i)\cos h(\lambda_s^{I} h_i) - \lambda_s^{I} h_i\\
&\Omega_{s3}^{I} = \Omega_{s5}^{I} = \Omega_s(\lambda_s^{I'} h_i),\ \Omega_{s4}^{I} = \Omega_{s6}^{I} = \Omega_s^{*}(\lambda_s^{I'} h_i)\\
&(I = I, II, III;\quad i = 1, 2, 3)
\end{aligned}$$

Substituting Eqs. (10) and (12) into Eqs. (6) and (7), $48 \times N$ simultaneous equations are obtained, where N denotes the number of terms in the Fourier series. By solving the $48 \times N$ simultaneous equations, the unknown coefficients are determined. Using the determined coefficients, the stress and displacement components of each finite strip in the plane strain state are obtained.

3. EXPERIMENTAL METHOD

Figure 3 shows the dimensions of specimens used in strain measurement and rupture tests. Adherends were made of aluminum alloy (A5052, Japan Industrial Standard) and mild steel (SS400, JIS) and the adhesive used was epoxy resin EA9430, Dexter Corporation. Table I

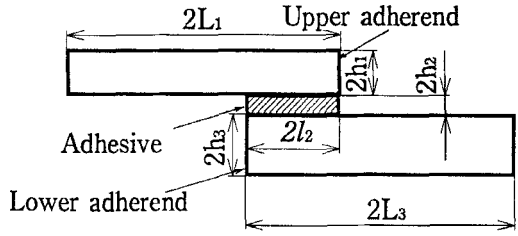

$2L_1$	$2h_1$	$2l_2$	$2h_2$	$2L_3$	$2h_3$
210	3, 6	18.8	0.1	210	3, 6
$2l_1$=127	1.6			$2l_1$=127	1.6

FIGURE 3 Dimensions of specimens used in strain measurement and rupture tests (units = mm).

TABLE I Mechanical properties of adherends and adhesive used in the experiments

	Adherend (*A*5052)	*Adherend* (*SS*400)	*Adhesive* (*EA*9430)
E(GPa)	69.69	200.4	1.770
ν	0.314	0.219	0.370
σ_y(MPa)	261.7	424.7	30.38

σ_y: yield stresses of the materials.

shows the properties of the materials (Young's modulus, E, Poisson's ratio, ν, and yield stress, σ_y) used in the experiments. The dimensions of the adherend specimens used in the experiments are as follows: the adherend length $2L_1 = 2L_3 = 210$ mm, the thickness $2h_1 = 2h_3 = 3$ and 6 mm and the width is held constant at 25.4 mm. The adhesive thickness, $2h_2$, shown in Figure 3 is held constant at 0.1 mm. A surface degreasing procedure was used in preparing the adhered surfaces for bonding. At first, the bonded surfaces of steel adherends were ground and those of aluminum adherends were lapped, and then the bonded surfaces were degreased by butanone, and joints were bonded using the epoxy resin. After assembly, the joints were cured in an oven at 60°C for 2 hours and at room temperature for 24 hours. Uniaxial strain gauges were attached to the lower surface of the upper adherend and the upper surface of the lower adherend near the edges of the adhesive. The orientation of the strain gages is perpendicular to the interfaces. Figure 4 shows a schematic experimental setup. By applying

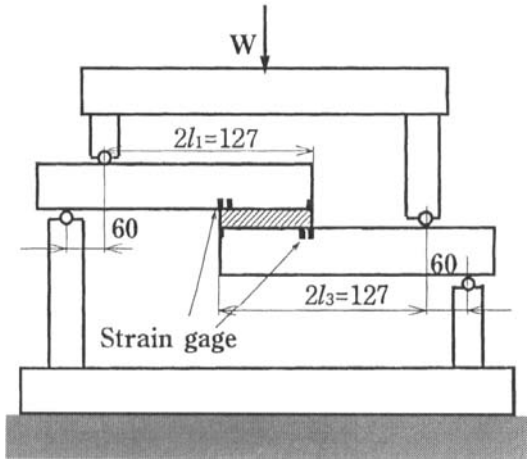

FIGURE 4 Schematic apparatus in strain measurement and rupture tests (units = mm).

a compression, W, which was measured by a load cell, a bending moment of $M = W/2 \times 60$ occurred. Table II describes the seven types of joint specimens and their dimensions. In the experiments, the lap length and the adherend thickness were varied as described in Table II. The lap length, $2l_2$, was held constant at 18.8 mm while the adherend lengths, $2l_1$ and $2l_3$, were held constant at 127 mm.

In addition, in order to measure the material properties of the adhesive, six dog-bone specimens were made from the EA9430 adhesive resin. The gauge length of the specimens was 70 mm, the width was 25.4 mm and the thickness was 3 mm. The curing process for the specimens is the same as that for the joint specimens.

TABLE II Types of speciments used in the experiments

Joint Symbol	*Material*	*Modulus ratio*(E_1/E_3)	h_1 (*mm*)	h_3 (*mm*)	*Lap-length ratio*(l_2/l_1)
(Al-St)$_1$	A5052-SS400	0.348	3	3	0.148
(Al-Al)$_1$	A5052-A5052	1	3	3	0.148
(Al-St)$_2$	SS400-A5020	2.867	3	3	0.148
(Al-Al)$_2$	A5052-A5052	1	1.6	6	0.148
(Al-Al)$_3$	A5052-A5052	1	3	6	0.148
(Al-Al)$_4$	A5052-A5052	1	6	3	0.148
(Al-Al)$_5$	A5052-A5052	1	6	1.6	0.148

4. RESULTS OF THEORETICAL ANALYSIS

In the numerical calculations, the stress components at the interfaces were computed by choosing the number of terms in the series as 100 and 200. It was noted that the difference in corresponding stress components between the cases of 100 and 200 terms was less than 1%, so that the convergnece was satisfactory. The numerical calculations were, therefore, carried out by using 100 terms in the series.

4.1. Effect of the Young's Modulus Ratio E_3/E_1 between the Upper and Lower Adherends on the Interface Stress Distributions

Figure 5 shows the effect of the Young's, moduli ratio, E_3/E_1, on the stress distributions of σ_x, σ_y and τ_{xy} and the maximum principal stress,

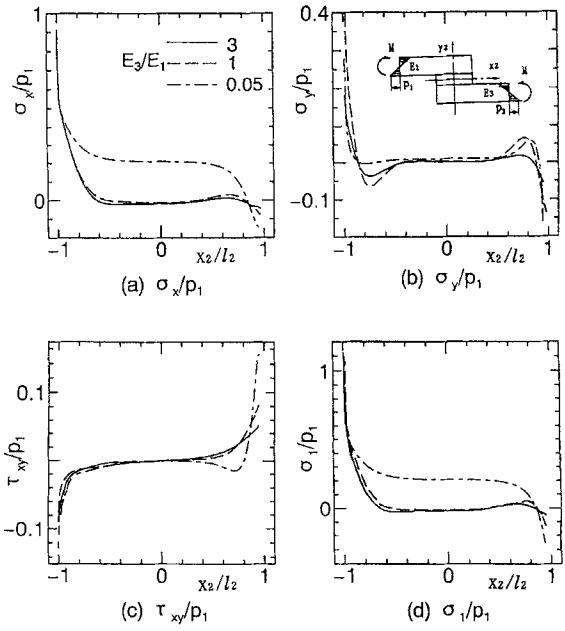

FIGURE 5 Effect of Young's modulus ratio, E_3/E_1, of the adherends on the stress distribution at the upper interface ($y_2 = -h_2$)($E_1 = 70\,\text{GPa}$, $E_2 = 3.5\,\text{GPa}$, $\nu_1 = \nu_3 = 0.3$, $\nu_2 = 0.38$, $2h_1 = 2h_3 = 3\,\text{mm}$, $2h_2 = 1\,\text{mm}$, $2l_1 = 2l_3 = 60\,\text{mm}$, $2l_2 = 40\,\text{mm}$).

σ_1, at the upper interface of the adhesive ($y_2 = h_2$). The value of E_3/E_1 was chosen as 3, 1 and 0.05, while the ratio E_2/E_1 was held constant at 0.05. The ordinates are the normalized stress components and the abscissa is the normalized distance. Figure 6 shows the stress distributions at the lower interface ($y_2 = -h_2$). In addition, a bending moment, M, acting on the end ($x_1 = -l_1$) of the upper interface is assumed to be applied in the region $|y_1| \leqq h_1$ as a linear distribution ($F(y_1) = p_1 y_1/h_1$) and a bending moment, M, is also assumed to be applied to the end ($x_3 = l_3$) of the lower interface in the region $|y_3| \leqq h_3$ as a linear distribution ($F(y_3) = -p_3 y_3/h_3$). It is assumed that the upper adherend thickness is equal to the lower one, that is, $h_1 = h_3$; therefore, the maximum distributive load intensity, p_1, applied in the region $|y_1| \leqq h_1$ is equal to the maximum distributive load intensity, p_3, applied in the region $|y_3| \leqq h_3$. In this study, the stress σ_x at the interface of the adhesive is examined because the fracture is thought to

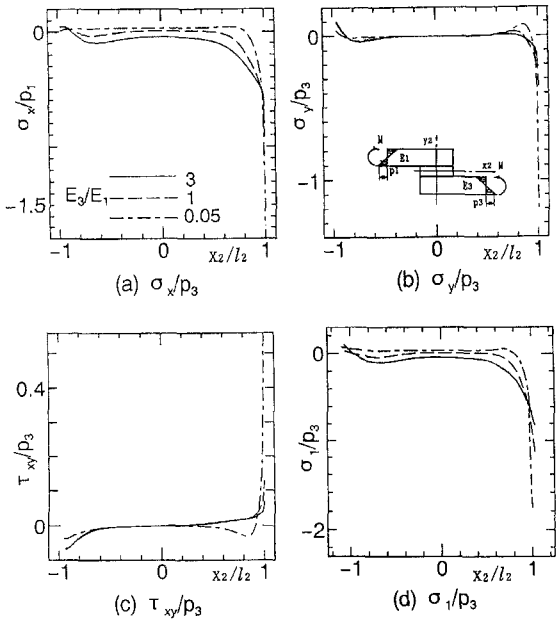

FIGURE 6 Effect of Young's modulus ratio, E_3/E_1, of the adherends on the stress distribution at the lower interface ($y_2 = -h_2$)($E_1 = 70$ GPa, $E_2 = 3.5$ GPa, $\nu_1 = \nu_3 = 0.3$, $\nu_2 = 0.38$, $2h_1 = 2h_3 = 3$ mm, $2h_2 = 1$ mm, $2l_1 = 2l_3 = 60$ mm, $2l_2 = 40$ mm).

initiate from the interface of the adhesive although the stress σ_x is different from that at the interface of the adherend. In Figure 5, it is found that the singular stresses occur at the edge of the upper interface ($x_2 = -l_2, y_2 = h_2$) and the effect of the ratio E_3/E_1 on the stress distributions along the upper interface is small. In Figure 6, it is seen that the stress components σ_x, σ_y and τ_{xy} at the edge of the lower interface ($x_2 = l_2, y_2 = -h_2$) increases as the ratio E_3/E_1 decreases. Because the singular stresses occur at the ends of the interfaces, the stresses up to 98% of the lap-length are described as one method. Notice the fact that when E_3/E_1 is varied as 3, 1 and 0.05, the ratio E_3/E_2 is varied as 60, 20 and 1 while E_1/E_2 is always held constant at 20, it could be concluded from the above results that the stress singularity at the edge of the interface is mainly related to the ratio of Young's modulus of the adherend to that of the adhesive. As the ratio of Young's modulus of the adherend to that of the adhesive decreases, the stress singularity at the edge of the interface increases. When the stiffness ratio is equal to 1, the stress singularity is most intensive (suppose that the stiffness ratio is always greater than 1, or equal to 1).

Figure 7 shows the normalized maximum principal stress, σ_1/p_1, near the edge of the upper interface ($x_2 = -l_2, y_2 = h_2$) and σ_3/p_3 near the edge of the lower interface ($x_2 = l_2, y_2 = -h_2$) by using the singular stress parameters [16, 17]. The normalized maximum principal stress near the edge of the upper interface is expressed as the equation $\sigma_1/p_1 = Kr^{-\lambda}$ (Fig. 7(a)), where K is the intensity of singular stress, λ is the order of the singularity, and r is a distance from the edge and expressed by the equation $r = (2l_2 - x)/(2l_2)$, where x is a distance from the edge $x_2 = l_2$. It is seen that the differences in the values of K at the edge of the upper interface ($y_2 = h_2$) are very small and the values of K decreases as the ratio E_3/E_1 decreases, and the values λ are also little changed. The values of K are changed as 0.105, 0.104 and 0.098 and the values of λ are changed as 0.356, 0.358 and 0.355, respectively, as the ratios E_3/E_1 are changed as 3, 1 and 0.05. From Figure 7(b), it is seen that the values of K at the lower interface ($y_2 = -h_2$) increases as the ratio E_3/E_1 decreases that is, it increases as Young's modulus, E_3, decreases. In addition, it is found that the values of K at the upper and lower interfaces are the same for an adhesive joint of similar adherends ($E_3/E_1 = 1$). The value of λ at the lower interface ($y_2 = -h_2$) increases as the ratio decreases and is obtained as 0.316, 0.358 and 0.460, when

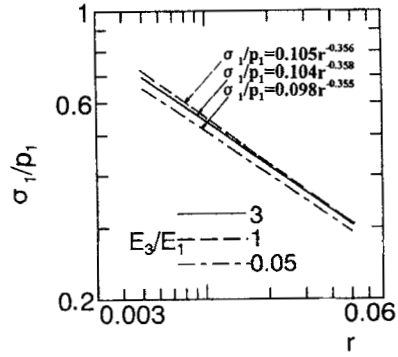

(a) σ_1/p_1 at the upper interface

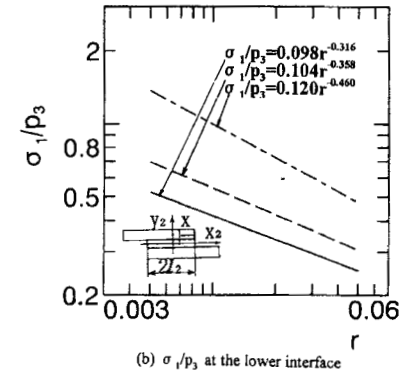

(b) σ_1/p_3 at the lower interface

FIGURE 7 Maximum principal stress σ_1/p_1 (σ_1/p_3) indicated in logarithmic scale.

the ratio E_3/E_1 is changed as 3, 1 and 0.05. On the other hand, the value of λ is obtained as 0.315, 0.355 and 0.465 from Bogy's theory [16, 17]. Fairly good agreement is seen between the present analytical results of the order λ and the results obtained from Bogy's theory.

4.2. Effect of the Adherend Thickness Ratio h_3/h_1 between the Upper and the Lower Adherends on the Interface Stress Distributions

The effect of the adherend thickness ratio, h_3/h_1, on the stress distributions at the interfaces ($y_2 = \pm h_2$) are analyzed by changing h_3/h_1 as 1, 2 and 3, where the value h_1 is held constant, and the ratio

E_3/E_1 is equal to 3 (E_3 = 210 GPa, E_2 = 3.5 GPa). The analysis shows that the effect of the ratio h_3/h_1 on the interface stress distributions ($y_2 = \pm h_2$) is small and the stress components $\sigma_x, \sigma_y, \tau_{xy}$ and the maximum principal stress, σ_1, increase slightly near the edge of the upper interface as the lower adherend thickness, h_3, increases. According to the results on the effects of Young's modulus ratio (section 3.1) and the thickness ratio (section 4.2) aforementioned, it can be concluded that the singular stresses increase at the interface of adherend with smaller rigidity. Figure 8 shows the effects of h_3/h_1 on

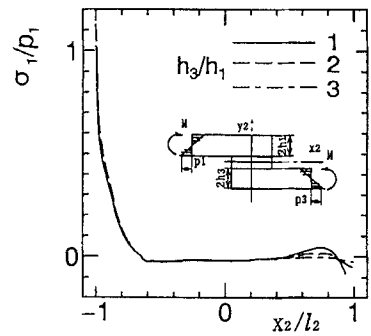

(a) σ_1/p_1 at the upper interface

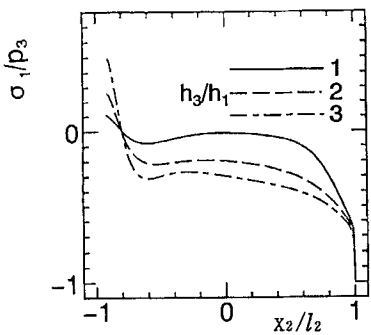

(b) σ_1/p_3 at the lower interface

FIGURE 8 Effect of the thickness ratio, h_3/h_1, of the adherends on the stress distribution at the interfaces ($y_2 = \pm h_2$)(E_1 = 70 GPa, E_2 = 3.5 GPa, E_3 = 210 GPa, $\nu_1 = \nu_3 = 0.3, \nu_3 = 0.38, 2h_1 = 3$ mm, $2h_2 = 1$ mm, $2l_1 = 2l_3 = 60$ mm, $2l_2 = 40$ mm).

the normalized maximum principal stress distributions, σ_1/p_1 and σ_1/p_3, at the interfaces ($y_2 = \pm h_2$).

4.3. Effect of the Length Ratio l_3/l_1 on the Stress Distributions at the Interfaces

The stress distributions at the interfaces are analyzed by changing the adherend length ratio, l_3/l_1, as 1.433, 1 and 0.614 when the length, l_2, is held constant. It is found that the stress components σ_x, σ_y and τ_{xy} are almost not affected when the ratio l_3/l_1 is changed. Figure 9 shows the

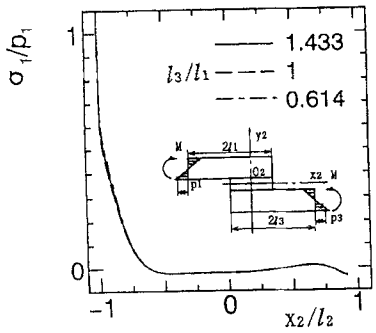

(a) σ_1/p_1 at the upper interface

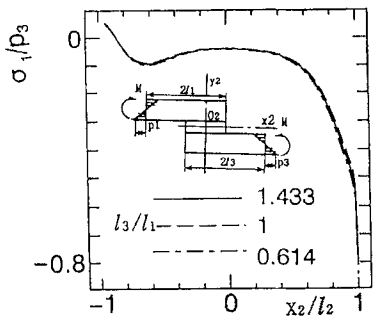

(b) σ_1/p_3 at the lower interface

FIGURE 9 Effect of the length ratio, l_3/l_1, of the adherends on the stress distribution at the interfaces ($y_2 = \pm h_2$)($E_1 = 70$ GPa, $E_2 = 3.5$ GPa, $E_3 = 210$ GPa, $\nu_1 = \nu_3 = 0.3$, $\nu_3 = 0.38$, $2h_1 = 3$ mm, $2h_2 = 1$ mm, $2l_1 = 2l_3 = 60$ mm, $2l_2 = 40$ mm).

effects of the adherend length ratio l_3/l_1 on the normalized maximum principal stress distributions, σ_1/p_1 and σ_1/p_3, at the interfaces ($y_2 = \pm h_2$). It can be concluded that for bending loading the effect of the adherend lengths on the interface stress distributions is small while the interface stress distributions are influenced by the adherend lengths when a single-lap adhesive joint of similar adherends is subjected to tensile loads [11].

5. COMPARISON OF THE ANALYTICAL RESULTS WITH THE EXPERIMENTAL AND THE FEA RESULTS

5.1. Comparison of Strain between the Analytical and Experimental Results

Figure 10 shows the comparison of the strain, ε_x, in the lower free surface of the upper adherend in the x_1 direction (Fig. 4) between the analytical (solid line) and the measured results (solid circle). A fairly good agreement is seen between the analytical and the measured results.

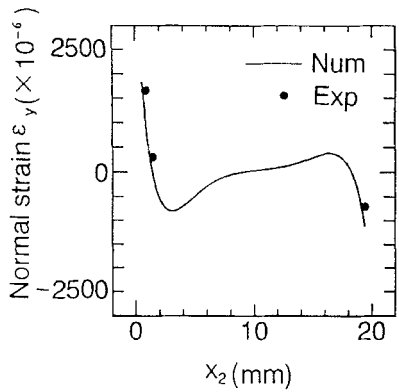

FIGURE 10 Comparison of strains between the numerical and the measured results at the upper interface ($y_2 = h_2$) (Upper adherend: A5052, lower adherend: SS400; $2l_1 = 2l_3 = 127$ mm, $l_2 = 18.8$ mm, $2h_1 = 2h_3 = 3$ mm, $2h_2 = 0.1$ mm, $M = 10.0$ KN mm).

5.2. Comparison of the Analytical Results with the FEM Results

In addition to the previous efforts, for verification of the present analysis, a two-dimensional finite element analysis (FEA) of a single-lap adhesive joint of dissimilar adherends subjected to an external bending moment is carried out. Figure 11 shows a model for the two-dimensional FEA. In the analysis, the upper and lower adherend thicknesses are chosen as 3 mm and the adhesive thickness as 0.05 mm. Young's modulus, E_1, and Poisson's ratio, ν_1, of the upper adherends are chosen as 70 GPa and 0.3, respectively, and those for the lower

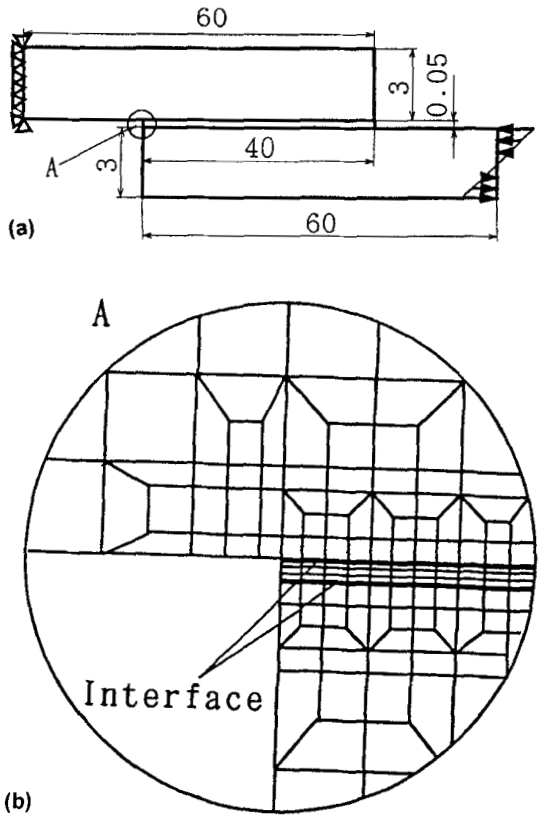

FIGURE 11 A model for FEA, (a) a model for FEA and the dimensions of the joint (mm); (b) Refined FEA meshes near the edge of the upper interface.

adherend as $E_3 = 210\,\text{GPa}$ and $\nu_3 = 0.3$, and those for the adhesive as $E_2 = 3.5\,\text{GPa}$ and $\nu_2 = 0.38$, respectively.

Since the effect of the size of elements near the interfaces, especially in the vicinity of the edges of the interfaces, is critical on the analytical results, the meshes are refined near the interfaces (Fig. 11(b)). The upper adherend is divided into 2452 quadrilateral elements, and the number of the elements for the lower adherend is the same as for the upper one. The adhesive is divided into 480 elements. The nodes and elements employed are 5594 and 5384, respectively. The FEA code employed was Marc. Figure 12 shows the comparison of the maximum principal stress distribution at the upper interface between the analytical and the FEA results. It can be seen that the analytical results are in fairly good agreement with the FEA results.

5.3. Comparisons of Joint Strength

It is not obvious how to choose a critical point and a mechanical variable according to which the strength of a single-lap adhesive joint

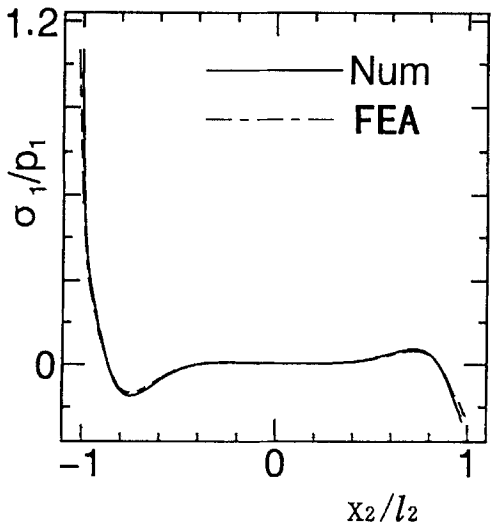

FIGURE 12 Comparison of maximum principal stress distribution at the upper interface ($y_2 = h_2$) between the analytical and FEA results ($E_1 = 70\,\text{GPa}, E_2 = 3.5\,\text{GPa}, E_3 = 210\,\text{GPa}, \nu_1 = \nu_3 = 0.3, \nu = 0.38, 2h_1 = 2h_3 = 3\text{mm}, 2h_2 = 0.05\,\text{mm}, 2l_1 = 2l_33 = 60\,\text{mm}, 2l_2 = 40\,\text{mm}$).

is determined. The left end of the upper interface is the most critical since the greatest stress exists at that point. However, it is not suitable to choose this left end of the upper interface as a critical point because the greatest stress at the point is singular and unstable. Calculation shows that in the vicinity of the end of the upper interface there is a position at which the stress level is quite stable. In this analysis, when the maximum principal stress at the point which belongs to the interface of the adhesive and is located at the position of $x_2/l_2 = -0.05$ reaches the fracture stress of the adhesive, the external bending moment is defined as the joint strength. The fracture stress of the adhesie was measured by using six dog-bone specimens, the dimensions of which are 160 (gauge length) × 25 (width) × 6(thickness) mm. These bulk specimens were made of adhesive resin EA9430. The cure process of the specimens is the same as that of the joint specimens. The average value was obtained as 43.2 MPa. Rupture tests were conducted 8 times for each type of specimen shown in Table II. A statistical procedure was applied to the experiment results and 95% of non-rupture joint strength was determined as the joint strength. The non-rupture joint strength was defined as the average value of the experimental results minus their average-square-root value. Figure 13 shows an example of the maximum principal stress distribution at the

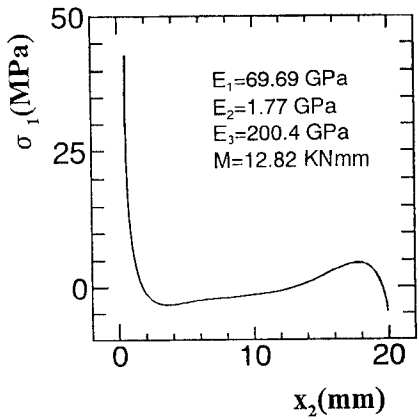

FIGURE 13 Maximum principal stress distribution at the upper interface of adhesive ($y_2 = h_2$) (Upper adherend: A5052, lower adherend: SS400; $2l_1 = 2l_3 = 127$ mm, $2l_2 = 18.8$ mm, $2h_1 = 2h_3 = 3$ mm, $2h_2 = 0.1$ mm).

upper interface under an external bending moment, M, of 12.82 KN mm for the specimen of type (Al-St)$_1$ shown in Table II, where the upper adherend is made of aluminum (E_1 = 69.69 GPa), the lower adherend is made of steel (E_3 = 200.4 GPa), the adherend thickness $2h_1 = 2h_3 = 3$ mm, the adhesive thickness $2h_2 = 0.1$ mm and the lap length $2l_2$ is 18.8 mm. For verification of the analysis, the finite element analysis (FEA) in elastic deformation was carried out for the joints shown in Table II. Table III shows the comparisons of the joint strength among the numerical (Analysis and FEA) and the experimental (Exp.) results. From Table III, it is found that joint strength increases as Young's modulus and the adherend thickness increases when the upper and lower adherends are similar. Also the joint strength will be increased with a decrease of the ratios E_3/E_1 when the adherends are dissimilar. Because as the ratio of E_3/E_1 decreases the singular stresses decrease (see Section 4.1), the joint strength will be enhanced. Although the effect of the adherend thickness ratio, h_3/h_1, on the normalized singular stresses is small (Section 4.2), the effect of the ratio h_3/h_1 on the joint strength is obvious. The joint strength obtained from the analysis is more conservative than that from the experiments because the analysis has been done in elastic deformation. However, the joint strength will be estimated by the analysis with a safety margin. It should be pointed out that the strength of single-lap adhesive joints subjected to external bending moments will depend on the yield stress of adherends, thus, elasto-plastic analysis will be needed in order to obtain the joint strength more precisely.

TABLE III Comparison of joint strength between the numerical FEA and experimental results (unit: KN mm)

Joint symbol	(*Al-St*)$_1$	(*Al-Al*)$_1$	(*Al-St*)$_2$	(*Al-Al*)$_2$	(*Al-Al*)$_3$	(*Al-Al*)$_4$	(*Al-Al*)$_5$
Analysis	12.82 (427)[a]	13.23 (441)	14.01 (476)	9.42 (314)	14.86 (495)	16.55 (551)	14.00 (466)
FEM	13.00 (433)	13.54 (451)	14.24 (474)	9.80 (326)	15.02 (500)	16.72 (557)	14.23 (474)
Experiment	17.28 (576)	18.37 (612)	22.05 (735)	13.5 (450)	20.01 (667)	22.15 (738)	18.26 (608)

[a] The values in parantheses indicate the load W shown in Figure 1(a) (unit:N).

6. CONCLUSIONS

This paper dealt with a stress analysis of single-lap adhesive joints of dissimilar adherends subjected to external bending moments. The following results were obtained.

(1) By replacing adherends and an adhesive with finite strips, a method for analyzing the stress distributions of single-lap adhesive joints of dissimilar adherends is demonstrated by using a two-dimensional theory of elasticity (plane strain).

(2) In the numerical calculations, the effect of Young's moduli ratio E_3/E_1, the thickness ratio h_3/h_1 and the length ratio l_3/l_1 between the dissimilar adherends on the stress distributions at the interfaces are clarified. It is found that when Young's modulus of the upper adherend is different from that of the lower adherend, stress components σ_x, σ_y and τ_{xy} near the edge of the interface of the adherend with smaller Young's modulus increase. The effect of the adherend thickness ratio on the normalized singular stresses at the edges of the interfaces is small. It is found that the stress components σ_x, σ_y and τ_{xy} near the edge of the interface of the adherend with smaller thickness increase slightly as the ratio h_3/h_1 increases. The effect of the adherend lengths on the singular stresses are very small.

(3) Strain measurements and two-dimensional finite element analysis (FEA) of single-lap adhesive joints of dissimilar adherends were carried out. The analytical results are in fairly good agreement with the strain measurement and the FEA results. In addition, the strength of joints is evaluated by using the maximum principal stress, σ_1. Comparing with the experimental results, it is found that the joint strength can be estimated with a safety margin. The joint strength predicted by the present analysis is conservative.

Acknowledgement

The authors would like to acknowledge Prof. K. Hirashima of Yamanashi University for his advice regarding the paper.

References

[1] Goland, M. and Reissner, E., *J. Appl. Mech.* **11**, A17 (1944).
[2] Chen, D. and Cheng, S., *J. Appl. Mech.* **50**, 109 (1983).

[3] Adams, R. D., Chambers, S. H., Delstrother, P. J. A. and Peppiatt, N. A., *J. Strain Analysis* **8**, 52 (1973).
[4] Harris, J. A. and Adams, R. D., *Int. J. Adhesion and Adhesives* **4**, 65 (1984).
[5] Kinloch, A. J., *J. Materials Science* **15**, 2141 (1980).
[6] Oplinger, D. Y., *Int. J. Solids Structures* **31**, 2565 (1994).
[7] Tsai, M. Y. and Morton, J., Trans. of ASME, *J. Appl. Mech.* **61**, 712 (1994).
[8] Sawa, T., Nakano, Y. and Toratani, H., *J. Adhesion Sci. Technol.* **11**, 1039 (1997).
[9] Sawa, T. and Suga, S., *J. Adhesion Sci. Technol.* **10**, 1255 (1996).
[10] Chen, D. and Cheng, S., Trans. ASME, *J. Appl. Mech.* **57**, 78 (1990).
[11] Sawa, T., Temma, K., Nishigaya, T. and Ishikawa, H., *J. Adhesion Sci. Technol.* **9**, 215 (1995).
[12] Sawa, T. and Uchida, H., *J. Adhesion Sci. Technol.* **11**, 811 (1997).
[13] Sawa, T., Nakano, Y. and Temma, K., *J. Adhesion* **24**, 1 (1987).
[14] Liu, J. and Sawa, T., *J. Adhesion Sci. and Technol.* **12**, 795–812 (1998).
[15] Harada, K., Hamada, H. and Maekawa, Z., *J. Adhesion Sci. and Technol.* **10**, 1089 (1996).
[16] Bogy, D. B., Trans. of ASME, *J. Appl. Mech.* **38**, 377 (1971).
[17] Hattori, T., *JSME Int. J.* **34**, 326–331 (1991).

APPENDIX

Outline of the Present Analysis

In the analysis, the boundary conditions at the interfaces ($y_1 = -h_1, y_3 = h_3$) are mixed boundary conditions. The outline of the analysis for the mixed boundaries at $y_1 = -h_1$ is described as follows. The analysis for the interface ($y_3 = h_3$) is the same as that at $y_1 = -h_1$.

The mixed boundary conditions at the regions $y_1 = -h_1$ and $y_2 = h_2$ for the model shown in Figure 1 can be expressed as Eqs. (A1) to (A4).

$$\begin{aligned} \sigma_y^{\mathrm{I}} &= \sigma_y^{\mathrm{II}} \ (C_1 - l_2 \leqq x_1 \leqq C_1 + l_2, \ -l_2 \leqq x_2 \leqq l_2) \\ \sigma_y^{\mathrm{I}} &= 0 \ (y_1 = -h_1, \ -l_1 \leqq x_1 \leqq C_2 - l_2) \end{aligned} \tag{A1}$$

$$\begin{aligned} \tau_{xy}^{\mathrm{I}} &= \tau_{xy}^{\mathrm{II}} \ (C_1 - l_2 \leqq x_1 \leqq C_1 + l_2, \ -l_2 \leqq x_2 \leqq l_2) \\ \tau_{xy}^{\mathrm{I}} &= 0 \ (y_1 = -h_1, \ -l_1 \leqq x_1 \leqq C_1 - l_2) \end{aligned} \tag{A2}$$

$$u_{,x}^{\mathrm{I}} = u_{,x}^{\mathrm{II}} \ (C_1 - l_2 \leqq x_1 \leqq C_1 + l_2, \ -l_2 \leqq x_2 \leqq l_2) \tag{A3}$$

$$v_{,x}^{\mathrm{I}} = v_{,x}^{\mathrm{II}} \ (C_1 - l_2 \leqq x_1 \leqq C_1 + l_2, \ -l_2 \leqq x_2 \leqq l_2) \tag{A4}$$

In the present analysis, taking into consideration the stress continuity condition, Eq. (A1), that σ_y^{I} is equal to σ_y^{II} in the region

of $-l_2 \leqq x_2 \leqq l_2$ and is zero in the region of $-l_1 \leqq x_2 \leqq C_1 - l_2$, the stress σ_y^{II} is expanded into a Fourier series of the terms λ_t^{I} and $\lambda_t^{\mathrm{I}'}$ in the expanded region $-l_1 \leqq x_1 \leqq l_1$. Then, the expanded Fourier series of σ_y^{II} is equated to the stress σ_y^{I} which is obtained from the stress function X^{I}. Thus, the following Eqs. (A5) and (A6) are obtained.

$$\begin{aligned}
&\sum_{t=1}^{\infty}\Bigg[\sum_{n=1}^{\infty}A_{n1}^{\mathrm{II}}SCH_{nt1}^{\mathrm{II\,I}}-\sum_{s=1}^{\infty}B_{s1}^{\mathrm{II}}SC_{st1}^{\mathrm{II\,I}}\\
&\qquad-\sum_{n=1}^{\infty}A_{n6}^{\mathrm{II}}SCH_{nt6}^{\mathrm{II\,I}}-\sum_{s=1}^{\infty}B_{s6}^{\mathrm{II}}SC_{st6}^{\mathrm{II\,I}}\Bigg]\\
&\quad-\sum_{t=1}^{\infty}\Bigg[\sum_{n=1}^{\infty}A_{n1}^{\mathrm{I}}SCH_{nt7}^{\mathrm{I}}-B_{t1}^{\mathrm{I}}\\
&\qquad+\sum_{n=1}^{\infty}A_{n2}^{\mathrm{I}}SCH_{nt2}^{\mathrm{I}}+B_{t2}^{\mathrm{I}}\Bigg]=0
\end{aligned}\tag{A5}$$

$$\begin{aligned}
&\sum_{t=1}^{\infty}\Bigg[\sum_{n=1}^{\infty}A_{n1}^{\mathrm{II}}SSH_{nmt1}^{\mathrm{II\,I}}-\sum_{s=1}^{\infty}B_{s1}^{\mathrm{II}}SS_{smt1}^{\mathrm{II\,I}}\Big)\\
&\qquad-\sum_{n=1}^{\infty}A_{n6}^{\mathrm{II}}SSH_{nmt6}^{\mathrm{II\,I}}-\sum_{s=1}^{\infty}B_{s6}^{\mathrm{II}}SS_{smt6}^{\mathrm{II\,I}}\Big)\Bigg]\\
&\quad-\sum_{t=1}^{\infty}\Bigg[\sum_{n=1}^{\infty}A_{n1}^{\mathrm{I}}SSH_{nt5}^{\mathrm{I}}-B_{t5}^{\mathrm{I}}\\
&\qquad+\sum_{n=1}^{\infty}A_{n6}^{\mathrm{I}}SCH_{nt6}^{\mathrm{I}}+B_{t6}^{\mathrm{I}}\Bigg]=0
\end{aligned}\tag{A6}$$

Concerning the shear stress boundary condition, Eq. (A2), the following Eqs. (A7) and (A8) are obtained in the similar manner.

$$\begin{aligned}
&\sum_{t=1}^{\infty}\Bigg[\sum_{n=1}^{\infty}A_{n3}^{\mathrm{II}}TCH_{nt3}^{\mathrm{II\,I}}+\sum_{s=1}^{\infty}B_{s3}^{\mathrm{II}}TC_{st3}^{II\,I}\\
&\qquad+\sum_{n=1}^{\infty}A_{n8}^{\mathrm{II}}TCH_{nt8}^{\mathrm{II\,I}}-\sum_{s=1}^{\infty}B_{s8}^{\mathrm{II}}TC_{st8}^{\mathrm{II\,I}}\Bigg]\\
&\quad-\sum_{t=1}^{\infty}\Bigg[-\sum_{n=1}^{\infty}A_{n7}^{\mathrm{I}}TCH_{nt7}^{I}+B_{t7}^{\mathrm{I}}\\
&\qquad+\sum_{n=1}^{\infty}A_{n8}^{\mathrm{I}}TCH_{nt8}^{\mathrm{I}}-B_{t8}^{\mathrm{I}}\Bigg]=0
\end{aligned}\tag{A7}$$

$$\sum_{t=1}^{\infty}\left[\sum_{n=1}^{\infty}A_{n3}^{\mathrm{II}}TSH_{nmt3}^{\mathrm{II\,I}}+\sum_{s=1}^{\infty}B_{s3}^{\mathrm{II}}TS_{smt3}^{\mathrm{II\,I}}+\sum_{n=1}^{\infty}A_{n8}^{\mathrm{II}}TSH_{nmt8}^{\mathrm{II\,I}}-\sum_{s=1}^{\infty}B_{s8}^{\mathrm{II}}TS_{smt8}^{\mathrm{II\,I}}\right)\right]$$
$$-\sum_{t=1}^{\infty}\left[-\sum_{n=1}^{\infty}A_{n3}^{\mathrm{I}}TCH_{nt3}^{\mathrm{I}}+B_{t3}^{\mathrm{I}}+\sum_{n=1}^{\infty}A_{n4}^{\mathrm{I}}TCH_{nt4}^{\mathrm{I}}-B_{t4}^{\mathrm{I}}\right]=0 \tag{A8}$$

In order to satisfy the displacement boundary condition, Eq. (A3), the derivative of displacement u_x^{I} which is defined in the region $-l_1 \leqq x_1 \leqq l_1$ is expanded into Fourier series of the terms λ_t^{II} and $\lambda_t^{\mathrm{II}\prime}$ in the smaller region $-l_2 \leqq x_2 \leqq l_2$. Then, equating the expanded Fourier series of u_x^{I} to the expanded Fourier series of $u_{,x}^{\mathrm{II}}$, the following Eqs. (A9) and (A10) are obtained.

$$\sum_{t=1}^{\infty}\left[-\sum_{n=1}^{\infty}A_{n1}^{\mathrm{I}}UCH_{nt1}^{\mathrm{I\,II}}+\sum_{s=1}^{\infty}B_{s1}^{\mathrm{I}}UC_{st1}^{\mathrm{I\,II}}-\sum_{n=1}^{\infty}A_{n2}^{\mathrm{I}}UCH_{nt2}^{\mathrm{I\,II}}+\sum_{s=1}^{\infty}B_{s2}UC_{st2}^{\mathrm{I\,II}}+\sum_{s=1}^{\infty}B_{s3}^{\mathrm{I}}UC_{st3}^{\mathrm{I\,II}}+\sum_{s=1}^{\infty}B_{s4}^{\mathrm{I}}UC_{st4}^{\mathrm{I\,II}}-\sum_{n=1}^{\infty}A_{n5}^{\mathrm{I}}UCH_{nt5}^{\mathrm{I\,II}}+\sum_{s=1}^{\infty}B_{s5}UC_{st5}^{\mathrm{I\,II}}-\sum_{n=1}^{\infty}A_{n6}^{\mathrm{I}}UCH_{nt6}^{\mathrm{I\,II}}+\sum_{s=1}^{\infty}B_{s6}UC_{st6}^{\mathrm{I\,II}}+\sum_{s=1}^{\infty}B_{s7}^{\mathrm{I}}UC_{st7}^{I\,II}-\sum_{s=1}^{\infty}B_{s8}^{\mathrm{I}}UC_{st8}^{\mathrm{I\,II}}\right]$$
$$-\sum_{t=1}^{\infty}\left[-\sum_{n=1}^{\infty}A_{n1}^{\mathrm{I}}UCH_{nt1}^{\mathrm{I}}+B_{s1}^{\mathrm{I}}UC_{t1}^{\mathrm{I}}+\sum_{s=1}^{\infty}B_{s3}^{\mathrm{I}}UC_{st3}^{\mathrm{I}}\right]=0 \tag{A9}$$

$$\sum_{t=1}^{\infty}\Bigg[-\sum_{n=1}^{\infty}A_{n1}^{\mathrm{I}}USH_{nt1}^{\mathrm{I\,II}}+\sum_{s=1}^{\infty}B_{s1}^{\mathrm{I}}US_{st1}^{\mathrm{I\,II}}-\sum_{n=1}^{\infty}A_{n2}^{\mathrm{I}}USH_{nt2}^{\mathrm{I\,II}}+\sum_{s=1}^{\infty}B_{s2}US_{st2}^{\mathrm{I\,II}}+\sum_{s=1}^{\infty}B_{s3}^{\mathrm{I}}US_{st3}^{\mathrm{I\,II}}+\sum_{s=1}^{\infty}B_{s4}^{\mathrm{I}}US_{st4}^{\mathrm{I\,II}}-\sum_{n=1}^{\infty}A_{n5}^{\mathrm{I}}USH_{nt5}^{\mathrm{I\,II}}+\sum_{s=1}^{\infty}B_{s5}US_{st5}^{\mathrm{I\,II}}-\sum_{n=1}^{\infty}A_{n6}^{\mathrm{I}}USH_{nt6}^{\mathrm{I\,II}}+\sum_{s=1}^{\infty}B_{s6}US_{st6}^{\mathrm{I\,II}}+\sum_{s=1}^{\infty}B_{s7}^{\mathrm{I}}US_{st7}^{\mathrm{I\,II}}-\sum_{s=1}^{\infty}B_{s8}^{\mathrm{I}}US_{st8}^{\mathrm{I\,II}}\Bigg]-\sum_{t=1}^{\infty}\Bigg[\sum_{n=1}^{\infty}A_{n6}^{\mathrm{I}}USH_{nt6}^{\mathrm{I}}+B_{s6}^{\mathrm{I}}US_{t6}^{\mathrm{I}}+\sum_{s=1}^{\infty}B_{s8}^{\mathrm{I}}US_{st8}^{\mathrm{I}}\Bigg]=0 \tag{A10}$$

In the same way, the derivative of displacement $v_{,x}^{\mathrm{I}}$ is expanded into Fourier series in the region $-l_2 \leq x_2 \leq l_2$. Then, equating the expanded Fourier series of $v_{,x}^{\mathrm{I}}$ to the expanded Fourier series of $v_{,x}^{\mathrm{II}}$, the following Eqs. (A11) and (A12) are obtained.

$$\sum_{t=1}^{\infty}\Bigg[-\sum_{s=1}^{\infty}B_{s1}^{\mathrm{I}}VC_{st1}^{\mathrm{I\,II}}+\sum_{s=1}^{\infty}B_{s2}^{\mathrm{I}}VC_{st2}^{\mathrm{I\,II}}-\sum_{n=1}^{\infty}A_{n3}^{\mathrm{I}}VCH_{nt3}^{\mathrm{I\,II}}-\sum_{s=1}^{\infty}B_{s3}VC_{st3}^{\mathrm{I\,II}}+\sum_{n=1}^{\infty}A_{n4}^{\mathrm{I}}VCH_{nt4}^{\mathrm{I\,II}}-\sum_{s=1}^{\infty}B_{s4}^{\mathrm{I}}VC_{st4}^{\mathrm{I\,II}}+\sum_{s=1}^{\infty}B_{s5}^{\mathrm{I}}VC_{st5}^{\mathrm{I\,II}}-\sum_{s=1}^{\infty}B_{s6}VC_{st6}^{\mathrm{I\,II}}-\sum_{n=1}^{\infty}A_{n7}^{\mathrm{I}}VCH_{nt7}^{\mathrm{I\,II}}+\sum_{s=1}^{\infty}B_{s7}VC_{st7}^{\mathrm{I\,II}}$$

$$+\sum_{n=1}^{\infty} A_{n8}^{\mathrm{I}} VCH_{st8}^{\mathrm{I\,II}} + \sum_{s=1}^{\infty} B_{s8}^{\mathrm{I}} VCH_{st8}^{\mathrm{I\,II}}\Bigg]$$
$$-\sum_{t=1}^{\infty}\Bigg[\sum_{s=1}^{\infty} B_{s6}^{\mathrm{II}} VC_{st6}^{\mathrm{II}} \tag{A11}$$
$$-\sum_{n=1}^{\infty} A_{n6}^{\mathrm{II}} VCH_{nt6}^{\mathrm{II}} - B_{t8}^{\mathrm{II}} VC_{t8}^{\mathrm{II}}\Bigg] = 0$$

$$\sum_{t=1}^{\infty}\Bigg[-\sum_{s=1}^{\infty} B_{s1}^{\mathrm{I}} VS_{st1}^{\mathrm{I\,II}} + \sum_{s=1}^{\infty} B_{s2}^{\mathrm{I}} VS_{st2}^{\mathrm{I\,II}}$$
$$-\sum_{n=1}^{\infty} A_{n3}^{\mathrm{I}} VSH_{nt3}^{\mathrm{I\,II}} - \sum_{s=1}^{\infty} B_{s3} VS_{st3}^{\mathrm{I\,II}}$$
$$+\sum_{n=1}^{\infty} A_{n4}^{\mathrm{I}} VSH_{st3}^{\mathrm{I\,II}} - \sum_{s=1}^{\infty} B_{s4}^{\mathrm{I}} VS_{st4}^{\mathrm{I\,II}}$$
$$+\sum_{s=1}^{\infty} B_{s5}^{\mathrm{I}} VS_{st5}^{\mathrm{I\,II}} + \sum_{s=1}^{\infty} B_{s6}^{\mathrm{I}} VS_{st6}^{\mathrm{I\,II}} \tag{A12}$$
$$-\sum_{n=1}^{\infty} A_{n7}^{\mathrm{I}} VSH_{nt7}^{\mathrm{I\,II}} + \sum_{s=1}^{\infty} B_{s7} VS_{st7}^{\mathrm{I\,II}}$$
$$+\sum_{n=1}^{\infty} A_{n8}^{\mathrm{I}} VCH_{nt8}^{\mathrm{I\,II}} + \sum_{s=1}^{\infty} B_{s8}^{\mathrm{I}} VS_{st8}^{\mathrm{I\,II}}\Bigg]$$
$$-\sum_{t=1}^{\infty}\Bigg[\sum_{s=1}^{\infty} B_{s1}^{\mathrm{II}} VS_{st1}^{\mathrm{II}} - \sum_{n=1}^{\infty} A_{n3}^{\mathrm{II}} VSH_{st3}^{\mathrm{II}} - B_{t3}^{\mathrm{II}} VS_{t3}^{\mathrm{II}}\Bigg] = 0$$

where SCH_{nti}^{J}, SC_{sti}^{J}, SSH_{nti}^{J}, SS_{sti}^{J}, TCH_{nti}^{J}, TC_{sti}^{J}, TSH_{nti}^{J}, TS_{sti}^{J}, UCH_{nti}^{J}, UC_{sti}^{J}, USH_{nti}^{J}, US_{sti}^{J}, VCH_{nti}^{J}, VC_{sti}^{J}, VSH_{nti}^{J}, VS_{sti}^{J}, $SCH_{nti}^{\mathrm{II\,I}}$, $SC_{sti}^{\mathrm{II\,I}}$, $SSH_{nmti}^{\mathrm{II\,I}}$, $SS_{smti}^{\mathrm{II\,I}}$, $TCH_{nti}^{\mathrm{II\,I}}$, $TC_{sti}^{\mathrm{II\,I}}$, $TSH_{nmti}^{\mathrm{II\,I}}$, $TS_{smti}^{\mathrm{II\,I}}$, $UCH_{nti}^{\mathrm{I\,II}}$, $UC_{sti}^{\mathrm{I\,II}}$, $USH_{nti}^{\mathrm{I\,II}}$, $US_{sti}^{\mathrm{I\,II}}$, $VCH_{nti}^{\mathrm{I\,II}}$, $VC_{sti}^{\mathrm{I\,II}}$, $VSH_{nti}^{\mathrm{I\,II}}$, $VC_{sti}^{\mathrm{I\,II}}$ (J = I and II, $i = 1, 2, \ldots, 8$) and so on are constants which are expressed in Fourier expansions.